Rock Mech Rock Engng (2008) 41 (4), 539–562
DOI 10.1007/s00603-007-0152-9
Printed in The Netherlands

**Rock Mechanics
and Rock Engineering**

Fracture toughness analysis on cracked ring disks of anisotropic rock

By

C.-H. Chen[1], C.-S. Chen[1], J.-H. Wu[2]

[1] Department of Resources Engineering, National Cheng Kung University,
Tainan, Taiwan
[2] Department of Civil Engineering, National Cheng Kung University, Tainan, Taiwan

Received November 15 2006; Accepted August 8 2007;

Summary

This paper presents a combination of the Boundary Element Method (BEM) and the cracked ring test to determine the mixed-mode (I–II) fracture toughness of anisotropic rocks. The proposed BEM is used to accurately calculate the Stress Intensity Factors (SIFs) of a cracked anisotropic plate. An anisotropic Hualien marble of Taiwan with a distinct foliation was selected to conduct the cracked ring tests. Based on the measurement of the failure load during the test, the mixed-mode (I–II) fracture toughness can be determined. Experimental results show that the radius ratio, inclination and crack angle significantly affect the fracture toughness. The mode-I fracture toughness (K_{IC}) is shown to decrease with the increase in hole diameter, whereas the mode-II fracture toughness (K_{IIC}) increases with the increase in hole diameter when the crack angle β is equal to 0°. The experimental methods proposed have the advantage that the material is easily prepared, the test procedure is simple, and the cost is low.

Keywords: Boundary element method, cracked ring test, fracture toughness, anisotropic rock, stress intensity factor

Notation

r_o, r_i	outer and inner radius of the ring specimen, respectively
a	half crack length
b	distance from the crack tip to the disk center
t	specimen thickness
$a/(r_o - r_i)$	normalized crack length
F_I, F_{II}	normalized stress intensity factor of mode-I and mode-II, respectively
K_I, K_{II}	stress intensity factor of mode-I and mode-II, respectively

---

Correspondence: Chia-Hau Chen, Chao-Shi Chen, Department of Resources Engineering, National Cheng Kung University, 701 Tainan, Taiwan
e-mail: n4891117@mail.ncku.edu.tw, chencs@mail.ncku.edu.tw

K_{IC}, K_{IIC}	fracture toughness of mode-I and mode-II, respectively
W_f	failure loading
α	half loading angle
ρ	radius ratio (= inner to outer diameter of a ring specimen)
ψ	inclination angle
β	crack angle
ν	Poisson's ratio
E	Young's modulus
G	shear modulus

1. Introduction

In recent years, rock fracture mechanics has been applied as a possible tool for solving a variety of rock engineering problems including rock cutting, hydro-fracturing, explosive fracturing, underground excavation, and rock mass stability. Rock fracture mechanics is essentially extended from the Griffith theory (1920) and Irwin's modification (1957) which recognizes the importance of stress intensity near a crack tip. Irwin introduced the Stress Intensity Factors (SIFs) to express the stress and displacement field near a crack tip. The opening mode (mode-I), sliding mode (mode-II), and tearing mode (mode-III) are three basic crack modes in a fracture process because of the asymmetrical loading of the crack. The critical value of the SIFs is defined as the fracture toughness when crack propagation initiates. In addition, the fracture toughness can be defined as a measure of the ability of a material to resist the growth of a preexisting crack under stress. Thus, rock fracture toughness is the most fundamental parameter in fracture mechanics, and can be obtained by experimental procedures if the SIFs are known for a given body under a certain type and magnitude of loading.

In the laboratory, there are many testing methods suggested by the International Society for Rock Mechanics (ISRM) for determining the mode-I fracture toughness of isotropic rocks, such as Chevron Bend (CB) specimens method, Short Rod (SR) specimens method, Cracked Chevron Notched Brazilian Disk (CCNBD) method, and Cracked Straight Through Brazilian Disk (CSTBD) method. Disadvantages of these methods include complicated loading fixtures, complex sample preparation, limitations due to the isotropic behavior of rocks and to mode-I conditions only. Recently, investigations in linear elastic fracture mechanics have focused on fracture toughness determination for mixed-mode (I–II) and mode-II. In engineering, we often need to consider the problems of mixed-mode cracks. However, no suggested method has been accepted as the standard by the ISRM, even though a broad range of testing methods have been used to evaluate the fracture toughness parameters under mixed-mode (I–II) loading.

The fracture of brittle materials occurs at a shear stress approximately equal to the tensile fracture stress. Hence, it is important from an engineering point of view to study the combined mode-I and mode-II (mixed-mode I–II) as described by Awaji and Sato (1978), Atkinson et al. (1982), Lim et al. (1994), Chen et al. (1998b), and Al-Shayea et al. (2000). Therefore, consideration of mixed-mode (I–II) becomes significant in fracture toughness investigations. The major objective has been to determine the SIFs near the crack tip based on linear elastic fracture mechanics.

Whittaker et al. (1992) concluded that the following methods can be used to determine the SIF: (i) analytical methods (i.e. complex stress function, weight function, stress concentration, integral transformation), (ii) numerical methods (i.e. finite element, finite difference, boundary element, boundary collocation), (iii) experimental methods (i.e. photo-elastic, compliance, acoustic emission), and (iv) estimative methods (i.e. superposition). The numerical method is most commonly used among these methods.

The advantages of the boundary element method (BEM) over other numerical solution procedures (Brebbia, 1978) include (i) a reduced set of equations and dimensionality of a problem, (ii) a relatively small amount of data, (iii) proper modeling of infinite domains, (iv) no interpolation error inside the domain, and (v) a valuable representation for stress concentration problems. In short, the formulation of BEM is based on fundamental solutions that satisfy the governing differential equations, and the approximate variables required only on the boundary of the numerical solution of the boundary integral equation.

Application of the two-dimensional (2-D) elasticity problems of a circular ring with a cracked straight through specimen has been an important topic in fracture mechanics. Murakami and Nisitani (1975) presented the relationship of SIFs between the radius ratio and the crack for the cracked hollow spin disk. Webster et al. (1983) used BEM to determine the SIFs and the fatigue crack growth behavior in tubes. Leung et al. (1999) calculated the SIFs using the superposition principle. Niu et al. (2001) obtained the SIFs of mode-I and mode-II, and the energy release rate for crack extension using finite element analysis.

These researchers investigated the SIFs for isotropic materials that cannot satisfy the actual conditions for anisotropic rocks. For example, rock anisotropy affects the stability of underground excavations, surface excavations and foundations in civil engineering, the drilling, blasting and rock cutting in mining engineering, and is a critical factor for controlling borehole deviation, stability, deformation and failure in petroleum engineering. Therefore, to consider an anisotropic material is essential in many rock engineering problems.

To easily obtain the cracked ring disk, we often drilled a hole in the center of the Brazilian disk, and then generated the crack from the periphery of the hole. Specimens consisted of anisotropic Hualen marble of Taiwan. A hole was drilled at the center of each specimen to conduct the cracked ring test for measuring the fracture toughness. The variations of the SIFs of the marble with the inclination angle, the crack angle and the size of hole were investigated. In addition, the single domain BEM formulation was used to calculate the SIFs of a cracked anisotropic plate. Then, a combination of numerical analysis using the BEM and cracked ring specimen tests under diametral loading is presented for determining the normalized fracture toughness of anisotropic rocks under a mixed-mode (I–II) loading.

2. Theoretical background

2.1 Theoretical basis of the anisotropic disk specimen

Assume that a thin disk consists of a linearly elastic, homogeneous, continuous, and transversely isotropic material. As shown in Fig. 1, the thickness and radius are t and r_o, respectively. Let x, y, and z be three axes of a global Cartesian coordinate system; x

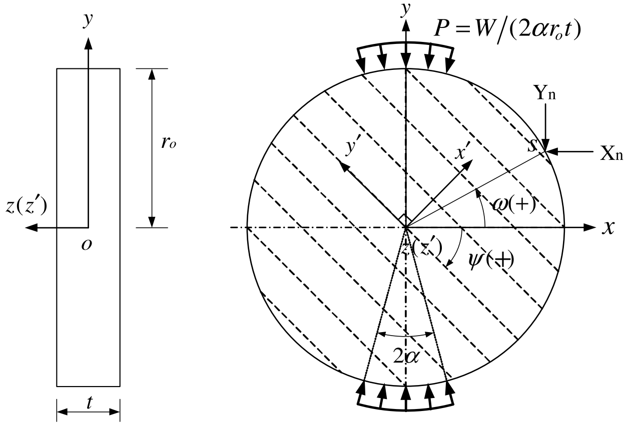

Fig. 1. Coordinate systems of the anisotropic disk specimen

and y are horizontal and vertical axes, respectively, while z is defined as the coordinate axis of the axle center direction of the disk.

Let Xn and Yn be the components of surface tractions in the x and y directions applied to the disk boundary. In addition, define a local coordinate system x', y', and z' as connected to the plane of transverse isotropy. The x'- and y'- axes are perpendicular and parallel to the plane, respectively. The z'-axis coincides with the z-axis of the global coordinate system. The inclination angle ψ is defined as the angle between the plane of transverse isotropy and the x-axis.

Lekhnitskii (1957) assumed that the disk is as follows: (i) has a plane of elastic symmetry parallel to its middle axis, (ii) is negligibly loaded by the surface forces of its thickness direction, and (iii) deforms insignificantly, then a generalized plane stress formulation of the disk can be used. The constitutive relation of the material in the x-y plane is expressed as follows:

$$\begin{Bmatrix} \varepsilon_x \\ \varepsilon_y \\ \gamma_{xy} \end{Bmatrix} = \begin{bmatrix} a_{11} & a_{12} & a_{16} \\ a_{12} & a_{22} & a_{26} \\ a_{16} & a_{26} & a_{66} \end{bmatrix} \cdot \begin{Bmatrix} \sigma_x \\ \sigma_y \\ \tau_{xy} \end{Bmatrix}, \tag{1}$$

where $a_{11}, a_{12}, \ldots, a_{66}$ are the compliance components dependent on the angle ψ and the elastic constants in the x', y', z' coordinate system.

Amadei (1996) proposed the following equations to calculate $a_{11}, a_{12}, \ldots, a_{66}$ for the geometry of Fig. 1:

$$\begin{aligned}
a_{11} &= \frac{\sin^4\psi}{E'} + \frac{\cos^4\psi}{E} + \frac{\sin^2 2\psi}{4}\left(\frac{1}{G'} - \frac{2\nu'}{E'}\right), \\
a_{12} &= \frac{\sin^2 2\psi}{4}\left(\frac{1}{E'} + \frac{1}{E} - \frac{1}{G'}\right) - \frac{\nu'}{E'}\left(\cos^4\psi + \sin^4\psi\right), \\
a_{16} &= \sin 2\psi\left[\left(\frac{\sin^2\psi}{E'} - \frac{\cos^2\psi}{E}\right) + \left(\frac{1}{2G'} - \frac{\nu'}{E'}\right)\cos 2\psi\right],
\end{aligned}$$

$$
\begin{aligned}
a_{22} &= \frac{\cos^4\psi}{E'} + \frac{\sin^4\psi}{E} + \frac{\sin^2 2\psi}{4}\left(\frac{1}{G'} - \frac{2\nu'}{E'}\right),\\
a_{26} &= \sin 2\psi\left[\left(\frac{\cos^2\psi}{E'} - \frac{\sin^2\psi}{E}\right) - \left(\frac{1}{2G'} - \frac{\nu'}{E'}\right)\cos 2\psi\right],\\
a_{66} &= \sin^2 2\psi\left(\frac{1}{E'} + \frac{1}{E} + \frac{2\nu'}{E'}\right) + \frac{\cos^2 2\psi}{G'}.
\end{aligned}
\tag{2}
$$

where E, E', ν, ν', and G' are five independent elastic constants of a transversely isotropic material. E and E' are the Young's modulus for tension (or compression) in the plane of transverse isotropy (y' or z' direction) and in a direction normal to it (x' direction), respectively; ν and ν' are the Poisson's ratios characterizing the lateral strain response in the plane of transverse isotropy to a stress acting parallel and normal to it, respectively. The G' is the shear modulus normal to the plane of transverse isotropy. Furthermore, the shear modulus G in the plane of transverse isotropy is equal to $E/(2(1+\nu))$.

If we neglect the body forces, the equilibrium equations are satisfied identically by introducing the Airy stress function F as follows:

$$
\sigma_x = \frac{\partial^2 F}{\partial y^2}, \qquad \sigma_y = \frac{\partial^2 F}{\partial x^2}, \qquad \tau_{xy} = -\frac{\partial^2 F}{\partial x \partial y}. \tag{3}
$$

The compatibility equation is given by

$$
\frac{\partial^2 \varepsilon_x}{\partial y^2} + \frac{\partial^2 \varepsilon_y}{\partial x^2} = \frac{\partial^2 \gamma_{xy}}{\partial x \partial y} \tag{4}
$$

Substituting Eqs. (1) and (3) into the Eq. (4), the strains ε_x, ε_y, γ_{xy} must satisfy the following differential equation:

$$
a_{22}\frac{\partial^4 F}{\partial x^4} - 2a_{26}\frac{\partial^4 F}{\partial x^3 \partial y} + (2a_{12} + a_{66})\frac{\partial^4 F}{\partial x^2 \partial y^2} - 2a_{16}\frac{\partial^4 F}{\partial x \partial y^3} + a_{11}\frac{\partial^4 F}{\partial y^4} = 0, \tag{5}
$$

the general solution of Eq. (5) depends on the roots, μ_i ($i = 1 \sim 4$), of the following characteristic equation:

$$
a_{11}\mu^4 - 2a_{16}\mu^3 + (2a_{12} + a_{66})\mu^2 - 2a_{26}\mu + a_{22} = 0. \tag{6}
$$

Lekhnitskii (1963) concluded that the roots of Eq. (6) are always either complex or imaginary. Let μ_1, μ_2 be the distinct roots of the characteristic equation, and $\bar{\mu}_1$, $\bar{\mu}_2$ their respective conjugate roots. As shown by Lekhnitskii, the first derivatives of F by x and y can be shown to be

$$
\begin{aligned}
\frac{\partial F}{\partial x} &= 2\mathrm{Re}[\phi_1(z_1) + \phi_2(z_2)],\\
\frac{\partial F}{\partial y} &= 2\mathrm{Re}[\mu_1\phi_1(z_1) + \mu_2\phi_2(z_2)],
\end{aligned}
\tag{7}
$$

where Re denotes the real part of the complex expression in the brackets, and $\phi_k(z_k)$ ($k = 1, 2$) are analytical functions of the complex variables $z_k = x + \mu_k y$, where μ_k are the roots of Eq. (6).

Combining Eqs. (3) and (7), the general expressions for the stress components under the loading with the disk specimens of the transverse isotropy are obtained as follows:

$$\begin{aligned}\sigma_x &= 2\mathrm{Re}[\mu_1^2\phi_1'(z_1) + \mu_2^2\phi_2'(z_2)],\\ \sigma_y &= 2\mathrm{Re}[\phi_1'(z_1) + \phi_2'(z_2)],\\ \tau_{xy} &= -2\mathrm{Re}[\mu_1\phi_1'(z_1) + \mu_2\phi_2'(z_2)],\end{aligned} \tag{8}$$

where $\phi_k'(z_k)$ ($k=1$, 2) are the first derivatives of $\phi_k(z_k)$ with respect to z_k.

Consider a uniform radial pressure $\sigma_r = P$ applied over the arcs $\pi/2 - \alpha < \omega < \pi/2 + \alpha$ and $3\pi/2 - \alpha < \omega < 3\pi/2 + \alpha$, as shown in Fig. 1. The stress distribution can be approximated by the following Fourier series in $\cos(n\omega)$ and $\sin(n\omega)$:

$$\sigma_r = A_0 + \sum_{n=1}^{N-1}(A_n \cos n\omega + B_n \sin n\omega), \tag{9}$$

with

$$A_0 = 2P\alpha/\pi, \quad A_n = \frac{2P}{\pi}\left(\frac{1+(-1)^n}{n}\right)\cos\frac{n\pi}{2}\sin n\alpha, \quad B_n = 0. \tag{10}$$

where n varies between 1 and $N-1$; ω is an angle defined in Fig. 1 which varies between 0 and 2π; and α is the half loading angle.

For the boundary conditions defined by Eqs. (9) and (10), no shear stress is applied along the boundary of the disk. The surface tractions X_n, Y_n depend on P only, and can be expressed as a Fourier series. Details of the calculation procedure for boundary conditions along the outer contour of the disk can be found in the paper of Chen et al. (1998a). Figure 1 shows that the loading angle is 2α, and P is equal to $W/(2\alpha r_o t)$ where W is the segmental load applied on the disk in the y direction.

The components of the stress field at any point (x, y) within the disk can be written as follows (Amadei et al., 1983):

$$\sigma_x = \frac{W}{2\pi r_o t}q_{xx}, \qquad \sigma_y = \frac{W}{2\pi r_o t}q_{yy}, \qquad \tau_{xy} = \frac{W}{2\pi r_o t}q_{xy}, \tag{11}$$

where q_{xx}, q_{yy}, and q_{xy} are three stress concentration factors, and they are dependent on the modulus of the elastic constants (E, E', ν, ν', and G'), the loading angle (2α), and the inclination angle (ψ).

Substituting Eq. (11) into Eq. (1), we obtain

$$\frac{2\pi r_o t}{W}\begin{Bmatrix}\varepsilon_x\\ \varepsilon_y\\ \gamma_{xy}\end{Bmatrix} = \begin{bmatrix}a_{11} & a_{12} & a_{16}\\ a_{12} & a_{22} & a_{26}\\ a_{16} & a_{26} & a_{66}\end{bmatrix}\cdot\begin{Bmatrix}q_{xx}\\ q_{yy}\\ q_{xy}\end{Bmatrix}. \tag{12}$$

2.2 2-D Boundary element analysis

From the theory of anisotropic linear elasticity in Sect. 2.1, the stress and displacement fields in a two-dimensional linear elastic, homogeneous and anisotropic medium can be formulated by two analytical functions $\phi_k(z_k)$, where the complex variables $z_k = x + \mu_k y$ ($k = 1, 2$), and μ_k are the roots of a characteristic equation, as shown in Eq. (6).

The general solution for the stress as shown in Eq. (8), and displacement components are (Sih et al., 1965):

$$\begin{aligned} u &= 2\mathrm{Re}[P_{11}\phi_1(z_1) + P_{12}\phi_2(z_2)], \\ v &= 2\mathrm{Re}[P_{21}\phi_1(z_1) + P_{22}\phi_2(z_2)], \end{aligned} \tag{13}$$

where

$$\begin{aligned} P_{1k} &= a_{11}\mu_k^2 + a_{12} - a_{16}\mu_k, \\ P_{2k} &= a_{12}\mu_k + a_{22}/\mu_k - a_{26} \quad (k = 1, 2). \end{aligned} \tag{14}$$

Sollero and Aliabadi (1993) suggested that the fundamental solution (called Green's function) of the tractions T_{ij}^* and the displacements U_{ij}^* can be given by the following Eqs. (15) and (16) when a source point (defined as s in Fig. 1) of the centralized load is applied on the infinite anisotropic plate, z_k^0 ($z_k^0 = x^0 + \mu_k y^0$):

$$T_{ij}^*(z_k, z_k^0) = 2\mathrm{Re}[Q_{j1}(\mu_1 n_x - n_y)A_{i1}(z_1 - z_1^0)^{-1} + Q_{j2}(\mu_2 n_x - n_y)A_{i2}(z_2 - z_2^0)^{-1}], \tag{15}$$

and

$$U_{ij}^*(z_k, z_k^0) = 2\mathrm{Re}[P_{j1}A_{i1}\ln(z_1 - z_1^0) + P_{j2}A_{i2}\ln(z_2 - z_2^0)] \quad (i, j = 1, 2), \tag{16}$$

where n_x and n_y are the outward normal vectors of the field points z_k, and $Q_{11} = \mu_1$, $Q_{12} = \mu_2$, $Q_{21} = Q_{22} = -1$. The complex coefficients A_{jk} are solutions of the following equation

$$\begin{bmatrix} 1 & -1 & 1 & -1 \\ \mu_1 & -\overline{\mu}_1 & \mu_2 & -\overline{\mu}_2 \\ P_{11} & -\overline{P}_{11} & P_{12} & -\overline{P}_{12} \\ P_{21} & -\overline{P}_{21} & P_{22} & -\overline{P}_{22} \end{bmatrix} \begin{bmatrix} A_{j1} \\ \overline{A}_{j1} \\ A_{j2} \\ \overline{A}_{j2} \end{bmatrix} = \begin{bmatrix} \delta_{j2}/(2\pi i) \\ -\delta_{j1}/(2\pi i) \\ 0 \\ 0 \end{bmatrix}, \tag{17}$$

where δ_{jk} is the Kronecker's delta function.

By the BEM formulation of Pan and Amadei (1996) for a cracked anisotropic material, the displacement integral equation is applicable to the outer boundary only, and its integral equation can be written as follows:

$$\begin{aligned} C_{ij}(z_{k,B}^0)u_j(z_{k,B}^0) &+ \int_{\Gamma_B} T_{ij}^*(z_{k,B}, z_{k,B}^0)u_j(z_{k,B})d\Gamma(z_{k,B}) \\ &+ \int_{\Gamma_C} T_{ij}^*(z_{k,C}, z_{k,B}^0)[u_j(z_{k,C+}) - u_j(z_{k,C-})]d\Gamma(z_{k,C}) \\ &= \int_{\Gamma_B} U_{ij}^*(z_{k,B}, z_{k,B}^0)t_j(z_{k,B})d\Gamma(z_{k,B}) \qquad z_{k,B}^0 \in \Gamma_B, \end{aligned} \tag{18}$$

where $i, j, k = 1, 2$; T_{ij}^* and U_{ij}^* are the Green functions of tractions and displacements; t_j and u_j are the boundary tractions and displacements; C_{ij} are quantities that depend on the geometry of the boundary and are equal to $\delta_{ij}/2$ for a smooth boundary; and z_k and z_k^0 are the field and source points on the boundary of the domain Γ ($\Gamma = \Gamma_B \cup \Gamma_C$). Γ_B and Γ_C are the no-crack boundary and crack surface, respectively. The subscript B

(or C) denotes the outer boundary (or the crack surface). And the other subscript $C+$ (or $C-$) indicates the positive (or negative) side of the crack.

In addition, the traction integral equation is collocated on one side of the crack surface only, and its result is shown as follows:

$$\begin{aligned}0.5t_j(z^0_{k,C}) + n_m(z^0_{k,C}) \int_{\Gamma_B} C_{lmik} T^*_{ij,k}(z^0_{k,C}, z_{k,B}) u_j(z_{k,B}) d\Gamma(z_{k,B}) \\ + n_m(z^0_{k,C}) \int_{\Gamma_C} C_{lmik} T^*_{ij,k}(z^0_{k,C}, z_{k,C})[u_j(z_{k,C+}) - u_j(z_{k,C-})] d\Gamma(z_{k,C}) \\ = n_m(z^0_{k,C}) \int_{\Gamma_B} C_{lmik} U^*_{ij,k} \times (z^0_{k,C}, z_{k,B}) t_j(z_{k,B}) d\Gamma(z_{k,B}) \qquad z^0_{k,C} \in \Gamma_{C+},\end{aligned} \tag{19}$$

where C_{lmik} is the fourth-order stiffness tensor, n_m is the unit outward normal to the contour path, and the gradient tensors $T^*_{ij,k}$ and $U^*_{ij,k}$ denote the derivative of T^*_{ij} and U^*_{ij} on the k direction.

For source points on the boundary Γ, neglecting body force, the traditional displacement boundary integral equation for linear elasticity can be expressed as:

$$c_{ij}(z^0_k) u_j(z^0_k) + \int_\Gamma T^*_{ij}(z_k, z^0_k) u_j(z_k) d\Gamma(z_k) = \int_\Gamma U^*_{ij}(z_k, z^0_k) t_j(z_k) d\Gamma(z_k). \tag{20}$$

Via the discretization equation, a linear system of algebraic equations can be solved for the unknown displacements u_j and tractions t_j on the boundary. The Cauchy singularity in boundary integral equation can be kept away from the rigid body motion method.

When the source points are located on the domain Ω, substituting the unknown (u_j, t_j), we obtain the boundary in Eq. (21). Thus, the displacements u_j are obtained at any internal point of the domain.

$$u_j(z^0_k) = \int_\Gamma U^*_{ij}(z_k, z^0_k) t_j(z_k) d\Gamma(z_k) - \int_\Gamma T^*_{ij}(z_k, z^0_k) u_j(z_k) d\Gamma(z_k). \tag{21}$$

Substitution of each displacement u_j of the intra-domain into the compatibility equation gives each strain intra-domain. And via the constitutive law relationship with stress–strain, each stress of the intra-domain is obtained.

2.3 Stress intensity factor and fracture toughness

In the applied mixed-mode load, the SIF of the crack tip depends on the relative crack displacement (RCD). Three node quadrilateral elements are employed to discretize both the boundaries and crack surfaces. The RCD on the crack surfaces can be approximated by their nodal values, and total displacement on each element can be expressed as follows:

$$\Delta u_i = \sum_{k=1}^{3} \phi_k \Delta u^k_i, \tag{22}$$

where the subscript $i\ (=1, 2)$ denotes the RCD component and the superscript $k\ (=1, 2, 3)$ denote the RCD at node positions $\xi = -2/3$, 0, 2/3, respectively, when the crack tip element at $\xi = -1$. The shape functions ϕ_k are introduced by Pan (1997) as follows:

$$\begin{aligned}
\phi_1 &= \frac{3\sqrt{3}}{8}\sqrt{\xi+1}\,[5 - 8(\xi+1) + 3(\xi+1)^2], \\
\phi_2 &= \frac{1}{4}\sqrt{\xi+1}\,[-5 + 18(\xi+1) - 9(\xi+1)^2], \\
\phi_3 &= \frac{3\sqrt{3}}{8\sqrt{5}}\sqrt{\xi+1}\,[1 - 4(\xi+1) + 3(\xi+1)^2].
\end{aligned} \tag{23}$$

Assume that the symmetric plane is normal to the z-axis (or z-axis is a two fold symmetry axis). For this case, the relation of the RCDs at a distance b behind the crack tip and the SIFs can be found as (Sih et al., 1965; Sollero and Aliabadi, 1993):

$$\begin{aligned}
\Delta u_1 &= 2\sqrt{\frac{2b}{\pi}}(H_{11}K_I + H_{12}K_{II}), \\
\Delta u_2 &= 2\sqrt{\frac{2b}{\pi}}(H_{21}K_I + H_{22}K_{II}),
\end{aligned} \tag{24}$$

where b is the distance from the crack tip to the disk center, and H_{ij} is material coefficient related to the following material elastic parameters in Eq. (25) (Pan and Amadei, 1996):

$$\begin{aligned}
H_{11} &= \mathrm{Im}\left(\frac{\mu_2 P_{11} - \mu_1 P_{12}}{\mu_1 - \mu_2}\right), \quad H_{12} = \mathrm{Im}\left(\frac{P_{11} - P_{12}}{\mu_1 - \mu_2}\right), \\
H_{21} &= \mathrm{Im}\left(\frac{\mu_2 P_{21} - \mu_1 P_{22}}{\mu_1 - \mu_2}\right), \quad H_{22} = \mathrm{Im}\left(\frac{P_{21} - P_{22}}{\mu_1 - \mu_2}\right),
\end{aligned} \tag{25}$$

where μ_i ($i = 1, 2$) are two roots of the characteristic Eq. (6). P_{ij} is the relative function of μ_i and the compliance components (a_{11}, a_{12}, a_{16}, a_{22}, a_{26}); Im denotes the imaginary part of a complex variable or function.

On the crack tip element, the RCD from the numerical calculation Eqs. (22) and (23) to the analytical Eqs. (24) and (25), then can be used to solve the SIFs of mode-I and mode-II (K_I and K_{II}). In this study, the fracture mode-I and mode-II are defined to be opening and sliding modes, respectively (Fig. 2). And the sign could be positive in compression (crack closing) or negative in tension (crack opening). Consider a cracked ring specimen under diametrical arc loading, as shown in Fig. 3. Let the inner radius, half crack length and distance from the crack tip to the disk center of the ring specimen be r_i, a and b, respectively. Then, the normalized SIFs (F_I and F_{II}) can be calculated as follows (Chen et al., 1998b):

$$F_I = \frac{K_I}{K_0}, \quad F_{II} = \frac{K_{II}}{K_0}, \tag{26}$$

where the regular factor $K_0 = W\sqrt{\pi b}/\pi r_o t$.

From Eq. (26), the maximum failure loading W_f is recorded, and the critical SIF of mode-I and mode-II (K_{IC} and K_{IIC}) can then be determined to denote the fracture toughness of the mixed-mode (I–II).

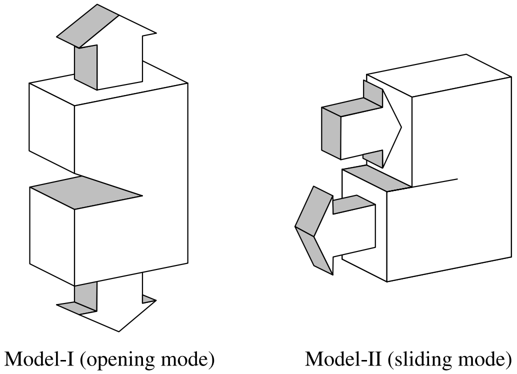

Fig. 2. The failure models of mode-I and mode-II

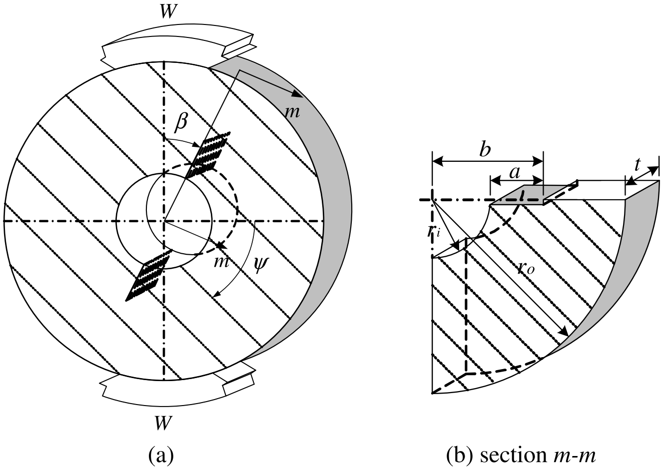

(a) (b) section *m-m*

Fig. 3. Cracked ring specimen of anisotropic rock under diametral loading

3. Numerical examples of SIFs for isotropic material

The geometry of the problems analyzed here is that of a cracked ring disk of radius r_o and thickness t with a crack of length a loaded by a pair of diametrical loading (Fig. 3). Outer and inner boundaries and the crack surface are discretized with 30, 10 continuous and 10 discontinuous quadratic elements, respectively (Fig. 4).

The Green's function and the particular solution were substituted into the boundary integral Eqs. (18–21), and the whole procedures were programmed in FORTRAN language to automatically determine the SIFs of the disk problems. In this section, three numerical examples are presented to verify the proposed BEM program.

Example 1. Isotropic Brazilian disk with a central crack

In this example, an isotropic cracked Brazilian disk with a central slant crack under a diametric loading is considered as shown in Fig. 5. In the boundary element division,

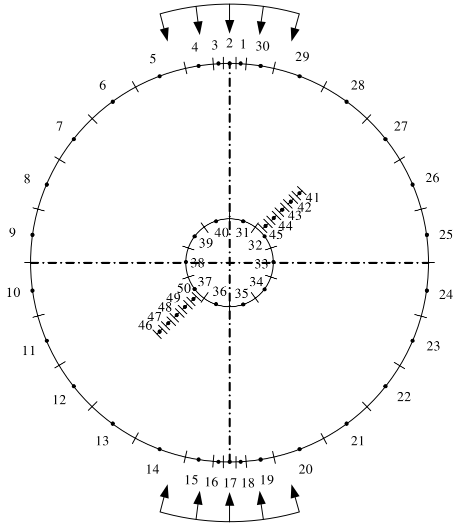

Fig. 4. Boundary element meshes for cracked ring disk

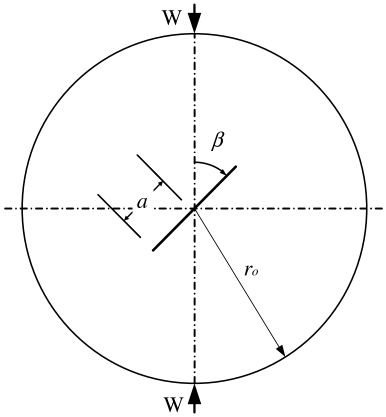

Fig. 5. A cracked Brazilian disk with inclined angle of crack β for $a/r_o = 0.5$

the outer boundary and the crack surface are discretized with 28 continuous and 10 discontinuous quadratic elements, respectively. The normalized SIFs analytically determined by Atkinson et al. (1982) using a continuous distribution dislocation method and simulated by Chen et al. (1998b) using the BEM combined with the J-integrate method were used to investigate the correctness of the new proposed BEM program.

Two cases are discussed as follows: (i) the normalized crack length a/r_o is equal to 0.5, and the crack angle β varies between 0 and 90°. As shown in Table 1, the simulation results correlate well with Atkinson's and Chen's solutions. (ii) The normalized crack length a/r_o varies between 0.1 and 0.7 when the crack angle is equal to 45°. Table 2 shows the normalized SIFs of cracks having different orientations from vertical to horizontal, and different lengths from short to long.

Table 1. Normalized SIFs of isotropic Brazilian disk with the crack angle β ($a/r_o = 0.5$)

β (deg)	Atkinson et al. (1982)		Chen et al. (1998b)		This study	
	K_I/K_0	K_{II}/K_0	K_I/K_0	K_{II}/K_0	K_I/K_0	K_{II}/K_0
0	−1.387	0	−1.339	0	−1.343	0
11.25	−0.970	1.340	−0.960	1.275	−0.952	1.281
22.5	−0.030	2.113	−0.074	2.061	−0.056	2.050
33.75	0.946	2.300	0.903	2.275	0.915	2.262
45	1.784	2.132	1.737	2.103	1.749	2.098
56.25	2.446	1.728	2.377	1.711	2.395	1.714
67.5	2.885	1.188	2.826	1.197	2.851	1.202
78.75	3.127	0.604	3.092	0.614	3.123	0.617
90	3.208	0	3.180	0	3.213	0

Table 2. Normalized SIFs with the normalized crack length ($\beta = 45°$)

a/r_o	Atkinson et al. (1982)		Chen et al. (1998b)		This study	
	K_I/K_0	K_{II}/K_0	K_I/K_0	K_{II}/K_0	K_I/K_0	K_{II}/K_0
0.1	1.035	2.010	1.020	1.968	1.018	1.965
0.2	1.139	2.035	1.116	1.995	1.116	1.992
0.3	1.306	2.069	1.272	2.036	1.277	2.029
0.4	1.528	2.100	1.484	2.069	1.492	2.065
0.5	1.784	2.132	1.737	2.103	1.749	2.098
0.6	2.048	2.200	2.020	2.148	2.039	2.139
0.7	–	–	2.337	2.213	2.364	2.224

Example 2. Isotropic ring disk with a single crack

The second example considers a ring disk with a vertical radial crack under a diametric loading, as shown in Fig. 6. The outer, inner boundaries and the single crack surface are discretized with 30, 10 continuous and 5 discontinuous quadratic elements, respectively (see Fig. 4). In this case, the radius ratio ρ, defined as r_i/r_o, is fixed to be

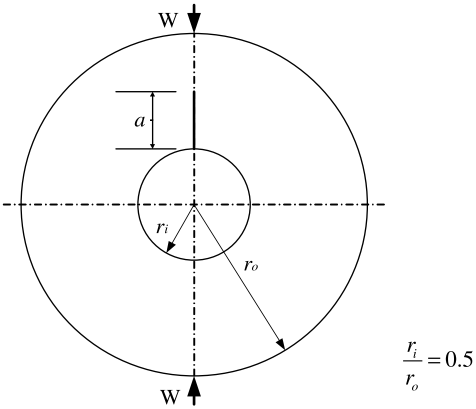

Fig. 6. A ring specimen with crack length a for $\rho = 0.5$

Table 3. Normalized SIF of mode-I (K_I/K_0) with the normalized crack length ($\rho = 0.5$)

$a/(r_o - r_i)$	Ahmad and Ashbaugh (1982)	This study
0.2	2.447	2.417
0.3	2.618	2.638
0.4	2.673	2.668
0.5	2.679	2.682
0.6	2.616	2.610
0.7	2.541	2.500
0.8	2.411	2.368

0.5, and the normalized crack length $a/(r_o - r_i)$ varies from 0.2 to 0.8. A comparison of the normalized SIF of mode-I determined by Ahmad and Ashbaugh (1982) using a finite element and by the proposed BEM in this study is shown in Table 3. The calculation results of our BEM program agree well with those determined by Ahmad and Ashbaugh (1982).

Example 3. Cracked isotropic ring disk

In the final example, consider a ring disk with a central straight notch under diametric loading, as shown in Fig. 7. The crack is described by 10 discontinuous quadratic elements with a total of 30 crack nodes. The normalized crack length $a/(r_o - r_i)$ is fixed to be 0.27 where a and r_i are 11 mm and 1.5 mm, respectively. Two normalized SIFs calculated with the BEM numerical solution are compared with the analytical solution proposed by Al-Shayea et al. (2000) and Atkinson et al. (1982).

In the research of Al-Shayea et al. (2000) a hole was drilled in the center of the Brazilian disk, and then the wire saw could easily pass through the drilled hole to generate the notch. However, the hole results in a singularity and must be neglected in the analytical solution. On the contrary, our numerical method can solve the problem

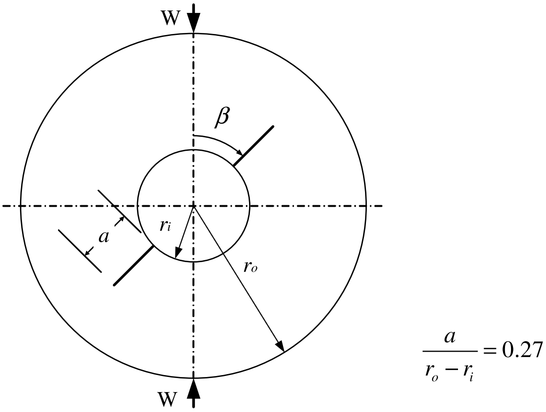

Fig. 7. A ring specimen with inclined angle of crack β for $a/(r_o - r_i) = 0.27$

Table 4. Normalized SIFs with the crack angle β ($a/(r_o - r_i) = 0.27$)

β (deg)	Al-Shayea et al. (2000)		Atkinson et al. (1982)		This study	
	K_I/K_0	K_{II}/K_0	K_I/K_0	K_{II}/K_0	K_I/K_0	K_{II}/K_0
0	−1.000	0	−1.136	0	−1.309	0
15	−0.682	1.085	−0.750	1.214	−0.926	1.231
30	0.137	1.791	0.200	1.956	0.099	1.710
45	1.137	1.931	1.306	2.069	1.433	1.928
60	2.000	1.554	2.246	1.656	2.437	1.640
75	2.545	0.847	2.850	0.906	3.070	1.028
90	2.726	0	3.056	0	3.153	0

including a hole. Table 4 shows that SIFs are relatively big when the hole exists. This case indicated that the influence of a hole is noticeable.

In addition, a pure tensile stress results along the x direction, when $\beta = 0°$, as the stress along the y direction vanishes. On the other hand, a pure compressive stress is present along the y direction when $\beta = 90°$. Consequently, the cracked isotropic disk can avoid the bi-axial state of stress in Brazilian disk and can accurately measure K_I with pure tensile or compressive stress.

4. Experimental investigation

4.1 Rock description

A Hualien marble from Eastern Taiwan with clear white–black foliations was selected to conduct both Brazilian and cracked ring tests. This marble is composed primarily of

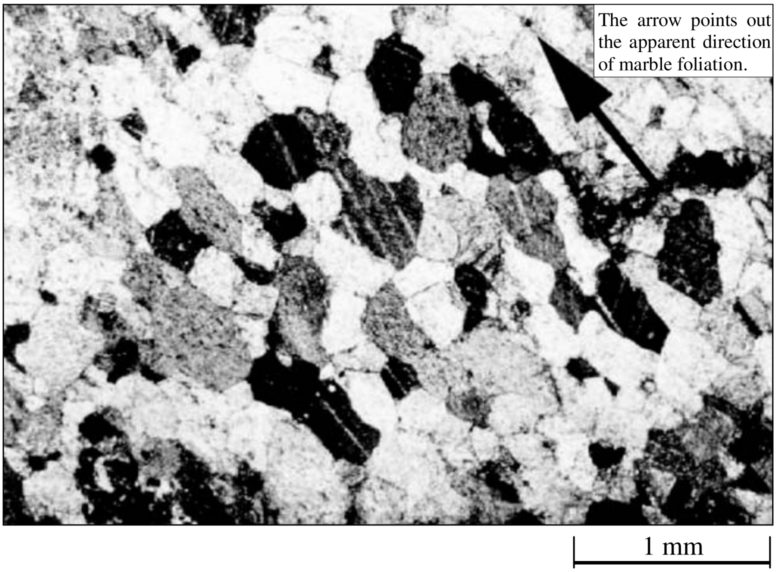

Fig. 8. Polarized micrograph of the Hualien marble

Table 5. Physical properties of the Hualien marble

Dry water content (%)	Specific gravity	Porosity (%)	Uniaxial compressive strength (MPa)		Tensile strength (MPa)			
			$\psi = 0°$	$\psi = 90°$	isotropic	transverse isotropic		
						$\psi = 15°$	$\psi = 45°$	$\psi = 75°$
0.12	2.66	0.24	84.69	56.70	7.27	11.07	7.47	4.56

dolomite and calcite, with an average grain size of 0.3 mm, as shown in Fig. 8. The polarized micrograph illustrates a thin cross section of fine rulings from deformational intra-crystalline gliding and preferred orientation. Because the marble exhibits a series of thin and parallel layers, it was assumed to be transversely isotropic, with the plane of transverse isotropy parallel to the apparent direction of rock symmetry.

Table 5 gives the physical properties of the marble including dry water content of 0.12%, specific gravity of 2.66, porosity of 0.24%, uniaxial compressive strength of 84.69 MPa ($\psi = 0°$) and 56.7 MPa ($\psi = 90°$). The tensile strength is 7.27 MPa for isotropic marble, and it is 11.07 MPa ($\psi = 15°$), 7.47 MPa ($\psi = 45°$) and 4.56 MPa ($\psi = 75°$) for transversely isotropic marble.

4.2 Sample preparation

Two types of experiments were conducted with the core samples taken from the blocks of marble.

In the first type of experiment, the elastic constants of the marble were determined by Brazilian test. A 74 mm diameter coring set was used to generate the samples. The cores were sliced and grinded into circular disks 11 mm thick using a high-speed circular saw and a grinding machine. Specimen preparation followed the ISRM Suggested Methods proposed by Bieniawski and Hawkes (1978). Three isotropic disks (BVE01, BVE02 and BVE03) and three transverse isotropic ones (BHE15, BHE45 and BHE75) having $\psi = 15°$, 45°, 75° were respectively prepared for the tests.

In the second type of experiment, cracked ring tests with 80 mm diameter and 11 mm thickness were prepared. The specimens were obtained from the marble blocks by drilling in the direction parallel to the apparent plane of isotropy. Three drills with diameters 1/4″, 1/2″, and 3/4″ were used to drill a hole in the center of each disk obtaining the following diameters: 6 mm, 12 mm, and 18 mm, respectively, to investigate the effect of a hole in determining the SIFs. Three ring specimens with $\rho = 0.075$, 0.15 and 0.225 (where ρ is the radius ratio, defined to be the ratio of the inner to the outer diameter) were obtained. A straight notch was formed at the center of the disks with different inclination angles ($\psi = 30°$, 60°) and crack angles ($\beta = 0°$, 45°) using a 0.4 mm steel wire saw. The wire was passed through the drilled hole and each crack length of 12 mm was made, referred to as types RFA30-A (or B), RFA60-A (or B), RFB30-A (or B), RFB60-A (or B), RFC30-A (or B) and RFC60-A (or B), respectively, for the cracked ring test.

4.3 Elastic constants of the Hualien marble

The five elastic constants of the transversely isotropic Hualien marble can be determined by the Brazilian tests using three specimens having different angles ($\psi = 15°$, $45°$, $75°$) to the plane of transverse isotropy (Chen et al., 1998a). In addition, a 45° strain gage rosette (Japan, TML type FRA-2-11 with factor of 2.11 and resistance of $120 \pm 0.5\Omega$) was attached to the center of each marble disk, as shown in Fig. 9, to measure strains. The specimens were placed between the steel loading jaws with a loading angle $2\alpha = 10°$, as suggested by the ISRM (1978). All the specimens

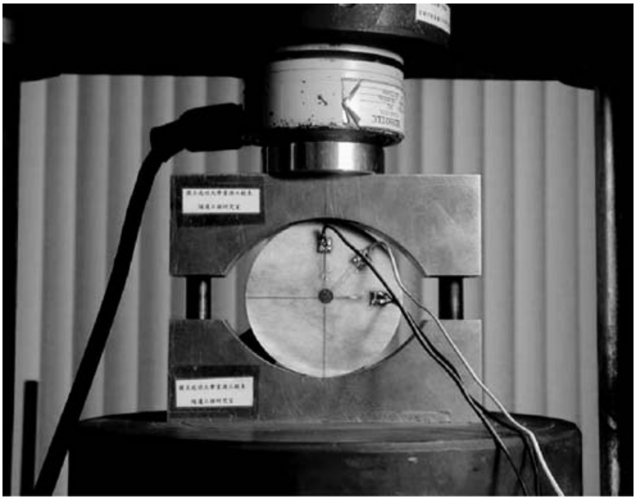

Fig. 9. Brazilian test device for determining elastic constants

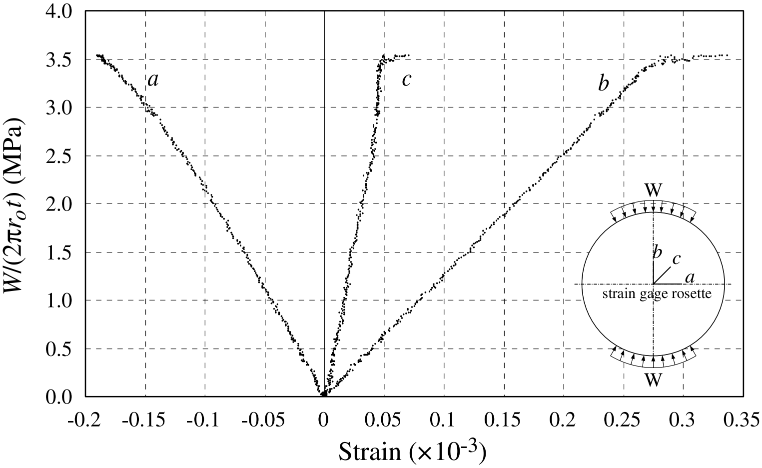

Fig. 10. Stress–strain curves of isotropic marble for sample BVE01

were loaded up to failure with a loading rate of 1 mm/min using a MTS-407 loading system.

Two sets of disk specimens were prepared to determine the elastic constants of the Hualien marble under diametral loading.

(i) One set of specimens, cored normal to the plane of transverse isotropy, was used to determine the isotropic constants E and ν. Figure 10 shows the typical response curves from the strain gage of specimen BVE01. From the stress–strain curves, the strain reaching 50% of the ultimate strength of Cure a was considered to be the transverse extensional strain, ε_x, negative. In the same process, the axial strain ε_y of Cure b was positive. For the plane of transverse isotropy of the medium, the stress concentration factors were set to be $q_{xx} = -2$, $q_{yy} = 6$ and $q_{xy} = 0$ with the small half loading angle α (7.5°) for the isotropic media.

The constitutive equations in generalized plane stress conditions from Eq. (12) can be written as follows:

$$\frac{2\pi r_o t}{W}\begin{Bmatrix}\varepsilon_x\\ \varepsilon_y\\ \gamma_{xy}\end{Bmatrix} = \begin{bmatrix}1/E & -\nu/E & 0\\ -\nu/E & 1/E & 0\\ 0 & 0 & 2(1+\nu)/E\end{bmatrix}\cdot\begin{Bmatrix}-2\\ 6\\ 0\end{Bmatrix}. \tag{27}$$

Hence, the solution of Eq. (27) results in the following expressions for the secant modulus of elasticity and Poisson's ratio:

$$E = \frac{16W}{2\pi r_o t(3\varepsilon_y + \varepsilon_x)}, \quad \nu = -\frac{3\varepsilon_x + \varepsilon_y}{3\varepsilon_y + \varepsilon_x}. \tag{28}$$

(ii) Another set of specimens was cored parallel to the plane of transverse isotropy and was used to determine the other three constants E', ν' and G'. Figure 11 illustrates typical stress–strain response of specimen BHE45 obtained from the central strain

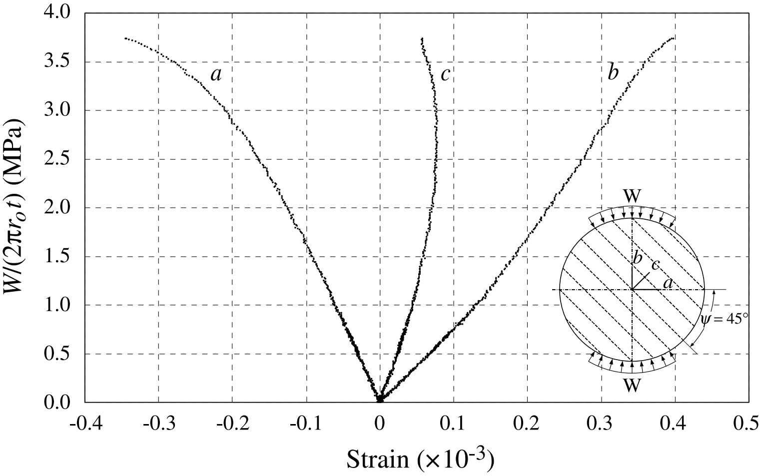

Fig. 11. Stress-strain curves of transversely isotropic marble for sample BHE45

gage. The strains at 50% of the ultimate strength were used as in case (i). Thus, the constitutive relations can be written as follows (Chen et al., 1998a):

$$\frac{2\pi r_o t}{W}\begin{Bmatrix}\varepsilon_x\\ \varepsilon_y\\ \gamma_{xy}\end{Bmatrix}-\frac{1}{E}\begin{Bmatrix}c_1\\ c_2\\ c_3\end{Bmatrix}=\begin{bmatrix}T_{11} & T_{12} & T_{13}\\ T_{21} & T_{22} & T_{23}\\ T_{31} & T_{32} & T_{33}\end{bmatrix}\cdot\begin{Bmatrix}1/E'\\ \nu'/E'\\ 1/G'\end{Bmatrix}, \tag{29}$$

where coefficients c_i and T_{ij} $(i, j = 1\text{–}3)$ depend on q_{xx}, q_{yy}, q_{xy} and ψ.

Lempriere (1968) and Amadei et al. (1987) concluded that the elastic constants for a transversely isotropic medium must satisfy the following thermodynamic constraints:

$$E, E'G \text{ and } G' > 0, \quad 1-\nu-2\frac{E}{E'}(\nu')^2 > 0, \tag{30}$$

Equation (29) is a nonlinear system with three unknowns ($1/E'$, ν'/E' and $1/G'$) which are constrained by the inequalities in Eq. (30).

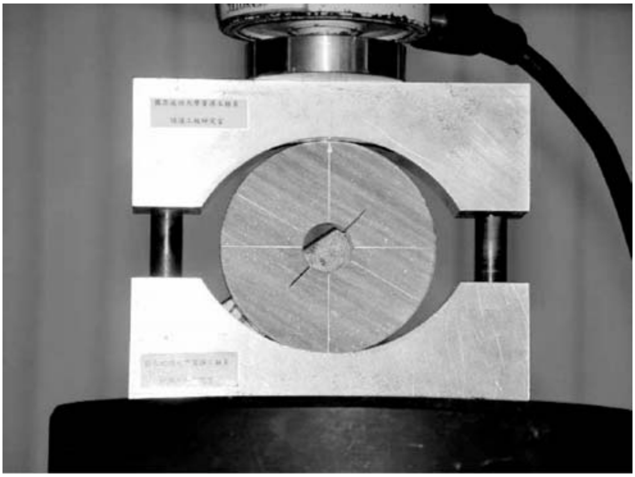

Fig. 12. Testing device of cracked ring disks

Table 6. Elastic constants in the plane of isotropy

Sample	D (mm)	t (mm)	$\mu\varepsilon_a\pi Dt/W$	$\mu\varepsilon_b\pi Dt/W$	$\mu\varepsilon_c\pi Dt/W$	E (GPa)	ν	G (GPa)
BVE01	74	11.45	−0.042	0.073	0.012	90.40	0.30	34.76
BVE02	74	11.78	−0.044	0.070	0.010	96.77	0.38	34.96
BVE03	74	11.82	−0.049	0.079	0.015	85.61	0.36	31.49
Average						90.93	0.35	33.74

* ε_a, ε_b and ε_c represent the strains in the x, y and 45° directions, respectively.

Table 7. Elastic constants in the plane of transverse isotropy

Sample	ψ	D (mm)	t (mm)	$\mu\varepsilon_a\pi Dt/W$	$\mu\varepsilon_b\pi Dt/W$	$\mu\varepsilon_c\pi Dt/W$	E' (GPa)	ν'	G' (GPa)
BHE15	15	74	12.24	−0.068	0.110	0.024	57.38	0.45	22.03
BHE45	45	74	12.34	−0.072	0.093	0.021	61.69	0.47	24.19
BHE75	75	74	12.24	−0.098	0.134	0.042	48.21	0.47	22.08
Average							55.76	0.46	22.77

Table 8. Elastic independent constants for Hualien marble

E (GPa)	E' (GPa)	ν	ν'	G' (GPa)	E/E'	G/G'
90.93	55.76	0.35	0.46	22.77	1.63	1.48

Finally, the elastic constants E, E', ν, ν' and G' are obtained from Eqs. (28) and (30), which completely describe the deformability of the transversely isotropic rock.

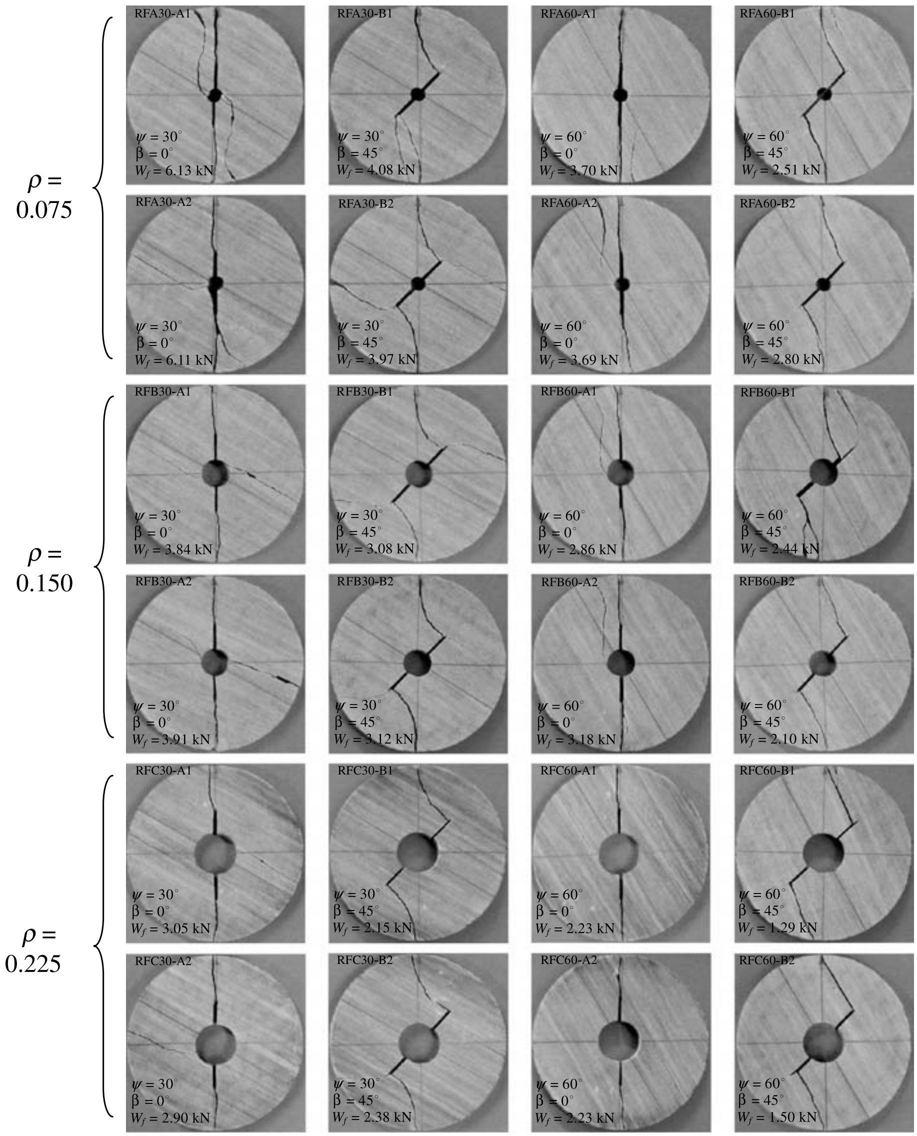

Fig. 13. Failure mode and failure loading of the cracked ring specimens

4.4 Cracked ring tests

A total of 24 mixed-mode cracked ring specimens were prepared with two inclination angles ($\psi = 30°$, $60°$), two crack angles ($\beta = 0°$, $45°$), and three specimen geometries ($\rho = 0.075$, 0.15, 0.225). Each specimen characteristics are listed in Tables 9, 10, and 11 for disks RFA, RFB, and RFC. The cracked ring specimens were taken to failure under an arc load with a loading angle of $2\alpha = 10°$ at a slow deformation rate of 1 mm/min using a 1 MN MTS-407 loading system, as shown in Fig. 12. The specimens used steel loading jaws to decrease the concentrated loading with the contact surface. Failure generally occurs within 5 min, while recording the maximum load of W_f. The mixed-mode (I–II) fracture toughness of each condition can be obtained using Eq. (26).

5. Experimental results and discussions

5.1 Five elastic constants by Brazilian test

The five independent elastic constants of the Hualien marble were determined by diametral loading on two sets of samples. The first set was loaded on the plane of transverse isotropy, and the strains were measured at 50% of the ultimate strength, where the failure stress was defined to be $W_f/2\pi r_o t$, as shown in Fig. 10. The elastic constants can be determined to be $E = 90.93$ GPa and $\nu = 0.35$, as shown in Table 6. In this table, ε_a and ε_b represent the strains measured in the x (horizontal) and y (vertical) directions, respectively.

The second set was loaded in the plane perpendicular to the plane of transverse isotropy (Fig. 11). The other three constants can be determined in Sect. 4.3 as $E' = 55.76$ GPa, $\nu' = 0.46$ and $G' = 22.77$ GPa, as shown in Table 7. Table 8 shows that the ratio E/E' of Hualien marble was equal to 1.63 (<2), and can be classified as a moderately anisotropic rock.

5.2 Fracture toughness by cracked ring test

Figure 13 shows the apparent failure modes for 12 cracked ring specimens (RFA30-A or B, RFA60-A or B, RFB30-A or B, RFB60-A or B, RFC30-A or B, RFC60-A or B). The following observations can be made: (i) the crack propagated along the loading direction when $\beta = 0°$, (ii) the RFC60-B1 and RFC60-B2 specimens failed initially

Table 9. Fracture toughness of cracked ring disk for type RFA ($\rho = 0.075$)

Sample	r_o (mm)	r_i (mm)	t (mm)	ψ (deg)	β (deg)	W_f (kN)	K_{IC} (MPa$\sqrt{\text{m}}$)	K_{IIC} (MPa$\sqrt{\text{m}}$)	$K_{IC,\text{avg}}$ (MPa$\sqrt{\text{m}}$)	$K_{IIC,\text{avg}}$ (MPa$\sqrt{\text{m}}$)
RFA30-A1	40	3	11.16	30	0	6.13	−1.52	0.17	−1.53	0.17
RFA30-A2	40	3	11.06	30	0	6.11	−1.53	0.17		
RFA60-A1	40	3	10.98	60	0	4.08	−0.84	0.11	−0.83	0.11
RFA60-A2	40	3	11.00	60	0	3.97	−0.82	0.11		
RFA30-B1	40	3	11.04	30	45	3.70	0.95	1.11	0.95	1.11
RFA30-B2	40	3	10.96	30	45	3.69	0.95	1.11		
RFA60-B1	40	3	10.94	60	45	2.51	0.80	0.82	0.84	0.86
RFA60-B2	40	3	11.02	60	45	2.80	0.88	0.90		

along the foliation with $\beta = 45°$, (iii) the maximum failure loading W_f decreased with the increase in the radius ratio; its value for $\beta = 0°$ is greater than for $\beta = 45°$, when $\psi = 30°$ or $60°$, and of $\psi = 30°$ is greater than $\psi = 60°$ when $\beta = 0°$ or $45°$ for each type of radius ratio, and (iv) the specimens did undergo after the first failure, and mostly located along the foliation because the load did not stop immediately.

Table 10. Fracture toughness of cracked ring disk for type RFB ($\rho = 0.150$)

Sample	r_o (mm)	r_i (mm)	t (mm)	ψ (deg)	β (deg)	W_f (kN)	K_{IC} (MPa$\sqrt{\text{m}}$)	K_{IIC} (MPa$\sqrt{\text{m}}$)	$K_{IC,\text{avg}}$ (MPa$\sqrt{\text{m}}$)	$K_{IIC,\text{avg}}$ (MPa$\sqrt{\text{m}}$)
RFB30-A1	40	6	11.00	30	0	3.84	−1.35	0.19	−1.38	0.19
RFB30-A2	40	6	10.84	30	0	3.91	−1.40	0.19		
RFB60-A1	40	6	10.96	60	0	3.08	−0.97	0.15	−0.97	0.15
RFB60-A2	40	6	11.06	60	0	3.12	−0.97	0.15		
RFB30-B1	40	6	10.98	30	45	2.86	0.69	1.08	0.73	1.14
RFB30-B2	40	6	11.00	30	45	3.18	0.76	1.20		
RFB60-B1	40	6	10.96	60	45	2.44	0.73	0.90	0.68	0.83
RFB60-B2	40	6	11.14	60	45	2.10	0.62	0.76		

Table 11. Fracture toughness of cracked ring disk for type RFC ($\rho = 0.225$)

Sample	r_o (mm)	r_i (mm)	t (mm)	ψ (deg)	β (deg)	W_f (kN)	K_{IC} (MPa$\sqrt{\text{m}}$)	K_{IIC} (MPa$\sqrt{\text{m}}$)	$K_{IC,\text{avg}}$ (MPa$\sqrt{\text{m}}$)	$K_{IIC,\text{avg}}$ (MPa$\sqrt{\text{m}}$)
RFC30-A1	40	9	10.92	30	0	3.05	−1.73	0.21	−1.67	0.21
RFC30-A2	40	9	11.18	30	0	2.90	−1.61	0.20		
RFC60-A1	40	9	10.74	60	0	2.15	−1.08	0.14	−1.13	0.15
RFC60-A2	40	9	10.88	60	0	2.38	−1.17	0.15		
RFC30-B1	40	9	11.04	30	45	2.23	−0.30	0.07	−0.30	0.07
RFC30-B2	40	9	11.04	30	45	2.23	−0.30	0.07		
RFC60-B1	40	9	11.00	60	45	1.29	−0.17	0.07	−0.19	0.08
RFC60-B2	40	9	10.84	60	45	1.50	−0.20	0.09		

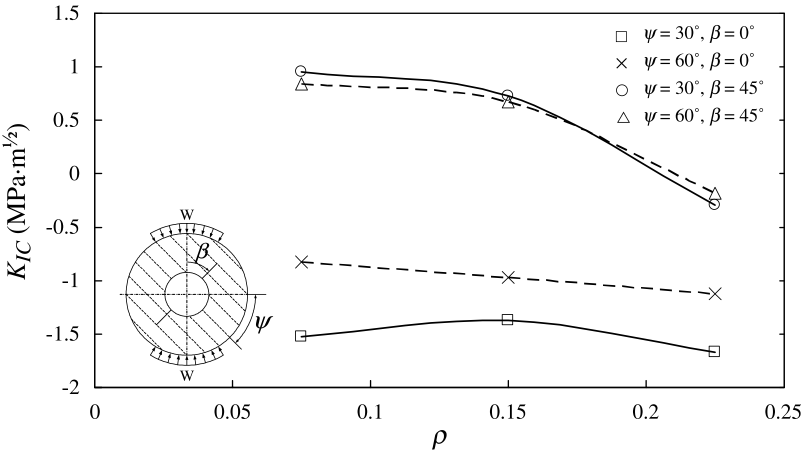

Fig. 14. Fracture toughness of mode-I vs. radius ratio ρ for different ψ and β

With the specimen geometry and the elastic constants of the marble known, a BEM analysis was conducted to determine the mixed-mode (I–II) fracture toughness. Once the failure loading was determined by the laboratory testing of cracked ring disks, the fracture toughness of the marble could be obtained. The laboratory test results for three ($\rho = 0.075$, 0.15, 0.225) are shown in Tables 9, 10, and 11, respectively. Obviously, the fracture toughness of mode-II is greater than mode-I ($K_{IIC} > K_{IC}$). It means that for anisotropic materials the effect of sliding is greater than that of opening.

Figures 14 and 15 show the variation of the fracture toughness of mode-I and mode-II, respectively, for the anisotropic marble with different values of ψ, β and ρ. For mode-I, the fracture toughness decreased with the increase in the diameter of the inner hole but increased in the radius ratio between 0.075 and 0.15. For mode-II, the fracture toughness increased with the increase in the diameter of hole when the angle

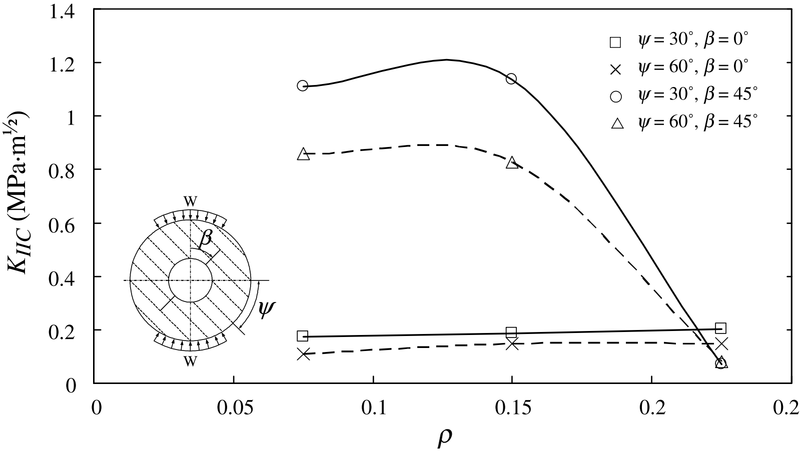

Fig. 15. Fracture toughness of mode-II vs. radius ratio ρ for different ψ and β

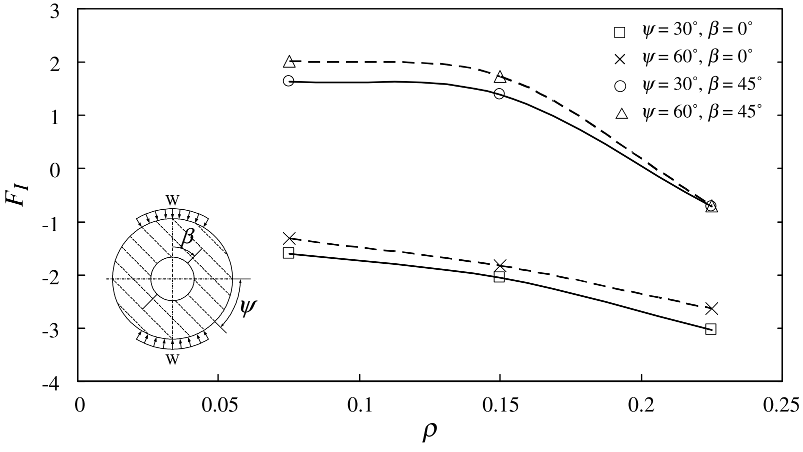

Fig. 16. Normalized SIF of mode-I vs. radius ratio ρ for different ψ and β

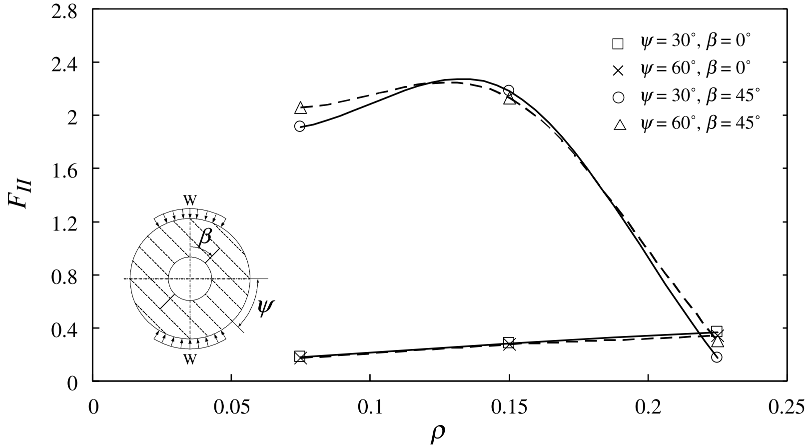

Fig. 17. Normalized SIF of mode-II vs. radius ratio ρ for different ψ and β

β was equal to 0°. However, the fracture toughness decreased in the value of the radius ratio between about 0.14 and 0.225 when the angle $\beta = 45°$. From Eq. (26), the normalized SIFs of mode-I and mode-II can be obtained in Figs. 16 and 17 to investigate the relationship between fracture toughness and regular factor. The analysis results show that the crack changes its orientation β from 0° to 45°, the F_I changes from negative to positive indicating crack closure. In addition, the SIF of mode-I (K_I) coincided with the one of mode-II (K_{II}) well for anisotropic materials when $\beta = 0°$ or 45°, and the K_I with pure tensile or compressive stress can be measured in the isotropic material when $\beta = 0°$ according to the numerical results of example 3.

6. Conclusions

This paper shows that the cracked ring disk under a diametral arc loading is a practical testing method for determining the mixed-mode fracture toughness of anisotropic rocks. This testing method has advantages due to convenient specimen preparation, simple apparatus and testing procedure, and no stress concentrations at the interface of the vertically loaded diameter and the outer boundary of disk. Combined with the BEM analysis and the cracked ring test, the mixed-mode SIFs can be successfully obtained. Numerical examples of SIFs for isotropic materials were conducted and good agreement was found.

The Hualien marble with clearly white–black foliations was selected to perform both Brazilian tests and cracked ring tests. A total of 6 Brazilian disks and 24 cracked ring disks were used to determine five elastic constants and the mixed-mode fracture toughness, respectively. The cracked ring specimen considered three values for the radius ratio (0.075, 0.15, 0.225), two different inclination angles (30°, 60°), and two crack angles (0°, 45°) to investigate the fracture toughness of mode-I (K_{IC}) or mode-II (K_{IIC}). The results obtained show that the K_{IC} decreased substantially with increased radius ratio. The K_{IIC} increased 37% with increased radius ratio and decreased with remaining 63% when the crack angle was equal to 45°, and another crack angle was slowly increased. Thus, the mixed-mode SIFs of anisotropic rocks are influenced by above mentioned three kinds of factors.

References

Al-Shayea NA, Khan K, Abduljauwad SN (2000) Effects of confining pressure and temperature on mixed-mode (I-II) fracture toughness of a limestone rock. Int J Rock Mech Min Sci 37: 629–643

Amadei B (1996) Importance of anisotropy when estimating and measuring in-situ stresses in rock. Int J Rock Mech Geo Abs 33: 293–325

Amadei B, Rogers JD, Goodman RE (1983) Elastic constants and tensile strength of anisotropic rocks. Proc 5th Congr. International Society Rock Mechanics, Melbourne, Australia, pp 189–196

Amadei B, Savage WZ, Swolfs HS (1987) Gravitational stresses in anisotropic rock masses. Int J Rock Mech Min Sci Geo Abs 24: 5–14

Atkinson C, Smelser RE, Sanchez J (1982) Combined mode fracture via the cracked Brazilian disk test. Int J Fracture 18: 279–291

Awaji H, Sato S (1978) Combined mode fracture toughness measurement by the disk test. J Eng Mater Tech 100: 175–182

Bieniawski ZT, Hawkes I (1978) Suggested methods for determining tensile strength of rock materials. Int J Rock Mech Min Sci Geo Abs 15: 99–103

Brebbia CA (1978) The boundary element method for engineers. Pentech Press, Plymouth and London

Chen CS, Pan E, Amadei B (1998a) Determination of deformability and tensile strength of anisotropic rock using Brazilian tests. Int J Rock Mech Min Sci 35: 43–61

Chen CS, Pan E, Amadei B (1998b) Fracture mechanics analysis of cracked discs of anisotropic rock using the boundary element method. Int J Rock Mech Min Sci 35: 195–218

Griffith AA (1920) The phenomena of rupture and flow in solids. Philos T Roy Soc A 221: 163–198

Irwin GR (1957) Analysis of stresses and strains near the end of a crack. J Appl Mech 24: 361–364

Lekhnitskii SG (1957) Anisotropic plates, translated by Tsai SW. Gordon and Breath, New York

Lekhnitskii SG (1963) Theory of elasticity of an anisotropic elastic body, translated by Fern P. Holden-Day Inc., San Francisco

Lempriere BM (1968) Poisson's ratios in orthotropic materials. J Am Institute Aeronaut Astronaut 6: 2226–2227

Leung AYT, Hu JD, Lo SH (1999) Green's function for general cracked ring problems. Int J Pres Ves Pip 76: 117–126

Lim IL, Johnston IW, Choi SK, Boland JN (1994) Fracture testing of a soft rock with semi-circular specimens under three point bending. Part 2 – Mixed mode. Int J Rock Mech Mining Sci Geo Abs 31: 199–212

Murakami Y, Nisitani H (1975) The stress intensity factors for the cracked hollow spin disk. Trans Jpn Soc Mech Eng 41: 2255–2264

Niu LS, Shi HJ, Robin C, Pluvinage G (2001) Elastic and elastic plastic fields on circular rings containing a v-notch under inclined loads. Eng Fract Mech 68: 949–962

Pan E (1997) A general boundary element analysis of 2-D linear elastic fracture mechanics. Int J Fracture 88: 41–59

Pan E, Amadei B (1996) Fracture mechanics analysis of 2D anisotropic media with a new boundary element method. Int J Fracture 77: 161–174

Sih GC, Paris PC, Irwin GR (1965) On cracks in rectilinearly anisotropic bodies. Int J Fracture 3: 189–203

Sollero P, Aliabadi MH (1993) Fracture mechanics analysis of anisotropic plates by the boundary element method. Int J Fracture 64: 269–284

Webster GA, Klintworth GC, Stacey A (1983) Stress intensity factors for cracked c-shaped and ring type test-pieces. J Strain Anal 18: 225–230

Whittaker BN, Singh RN, Sun G (1992) Rock fracture mechanics: principles, design and applications. Elsevier, New York